

Feature Enforcing PINN (FE-PINN): A Framework for Learning the Underlying-Physics to Resolve Unbalancing in the Objective Function Terms

Mahyar Jahaninasab^a, Mohamad Ali Bijarchi^{a,*}

^a Department of Mechanical Engineering, Sharif University of Technology, Tehran, Iran¹.

*Corresponding author: bijarchi@sharif.edu

Abstract:

In this study, we propose a new data-free framework, Feature Enforcing Physics Informed Neural Network (FE-PINN), to overcome the challenge of an imbalanced loss function in vanilla PINNs. The imbalance is caused by the presence of two terms in the loss function: the partial differential loss and the boundary condition mean squared error. A standard solution is to use loss weighting, but it requires hyperparameter tuning. To address this challenge, we introduce a process called “smart initialization” to force the neural network to learn only the boundary conditions before the final training in a designed process. In this method, clustered domain points are used to train a neural network with designed weights, resulting in the creation of a neural network called “Foundation network”. This results in a network with unique weights that understand boundary conditions. Then, additional layers are used to improve the accuracy. This solves the problem of an imbalanced loss function without further need for hyperparameter tuning. For 2D flow over a cylinder as a benchmark, smart initialization in FE-PINN is 574 times faster than hyperparameter tuning in vanilla PINN. Even with the optimal loss weight value, FE-PINN outperforms vanilla PINN by speeding up the average training time by 1.98. Also, the ability of the proposed approach is shown for an inverse problem. To find the inlet velocity for a 2D flow over a cylinder, FE-PINN is twice faster than vanilla PINN with the knowledge of optimal weight loss value for vanilla PINN. Our results show that FE-PINN not only eliminates the time-consuming process of loss weighting but also improves convergence speed compared to vanilla PINN, even when the optimal weight value is used in its loss function. In conclusion, this framework can be used as a fast and accurate tool for solving a wide range of Partial Differential Equations across various fields.

Keywords: Physics-Informed Neural Networks (PINNs), Physics-Informed Machine Learning, Loss weighting

1. Introduction

The rapid advancements in the field of artificial intelligence (AI) have inspired researchers to explore new ways to incorporate AI techniques into their respective fields. Raissi et al.'s pioneering work demonstrated the potential of neural networks as a powerful tool for solving partial differential equations (PDEs) [1]. The incorporation of a PDE loss term into the loss function, along with the mean squared error of predicting boundary conditions, led to the achievement of this solution. This breakthrough has since motivated many researchers to further investigate the use of deep learning techniques in various fields, including physics, finance, and engineering [2-4]. The vanilla form of PDEs solver, known as Physics-Informed Neural Networks (PINNs), represents a novel technique that has shifted attention from data-driven models to this emerging field [5-8]. The Vanilla PINN possesses remarkable versatility due to its mesh-free characteristics, enabling it to tackle a diverse range of challenges. It has proven its efficacy in different scenarios, ranging from forward to inverse problems [40]. For instance, it has successfully addressed the lid-driven cavity test case, which is governed by the incompressible Navier-Stokes equation [41]. Additionally, it has demonstrated its ability in handling multiphase problems [42], as well as scenarios involving flow past a cylinder and conjugate heat transfer [43]. These accomplishments solidify its status as a dependable approach for addressing various fluid mechanics dilemmas.

However, as research in this area has progressed, new and improved methods have been developed that build upon the original vanilla form. These methods involve modifications to various components of the vanilla form, such as the architecture [9], activation function [10], training method [11], sampling [12], and loss function [13]. One of the challenges in PINN is dealing with an imbalanced loss function, where the PDE loss term is more frequent than the boundary loss term. This issue can lead to a biased model that converges poorly. Lu et al. presented DeepXDE as a means to optimize the loss function of PINNs for PDEs. They proposed an approach called residual-based adaptive refinement (RAR), which incorporates supplementary collection points into areas characterized by high PDE residuals [34]. Nabian et al. introduced a collection point resampling strategy that utilizes importance sampling, relying on the loss function distribution to improve convergence [35]. Other studies focused on loss weighting problems with adaptive sampling strategies [36-39]. A limitation of these studies is the inability to effectively address the

imbalanced characteristics of the loss function and speed up the convergence as a result. These modifications can help researchers seeking to use this new tool as a potential replacement for traditional PDE-solver methods, as they can lead to faster convergence and improved result accuracy.

As such, the quest to enhance the convergence speed of PINN has become a prominent research topic, marking the beginning of a new era in the field. An enhanced, yet more expensive approach to speeding up the convergence speed of PINNs is through the use of decomposition methods. One example of using this technique to speed up the convergence of PINNs is the work of Alena Kopaničáková et al. They employed a decomposed neural network strategy by dividing it into sub-networks, with each sub-network being trained separately on a dedicated GPU [14]. While techniques such as decomposition methods can lead to a faster convergence rate, they require expensive resources for solving PDEs. This represents a potential drawback, even for simple problems. However, there are other approaches that can accelerate convergence speed without the need for such resources. One such approach is transfer learning [15]. Transfer learning is a powerful approach that entails leveraging knowledge from a pre-trained model to enhance the learning of another model [16]. Although recent advancements in transfer learning techniques have demonstrated their potential in training deep learning models [17-19], they are not widely applied to solve PDEs using neural networks. The fact that solutions to PDEs are specific to the problem being solved can make it difficult to effectively use transfer learning. The transferability of such tasks is considerably more challenging than that of classic tasks like image classification. Despite this difficulty, researchers have discovered novel applications of transfer learning for PINNs [20-22]. In addition to transfer learning, another technique that can help accelerate the convergence of neural networks is warm-up training. Warm-up training can help the model slowly adapt to the data and allows adaptive optimizers to compute correct statistics of the gradients [23]. Few studies have investigated the potential of warm-up training in this field [24]. Junjun Yan et al. utilized warm-up training to generate pseudo labels, which were subsequently employed in the main training loop [25]. Another popular approach to warm-up training involves initial training for a defined number of iterations with the ADAM optimizer, followed by another training loop with LBFGS, which leads to faster convergence in comparison to vanilla PINN [26].

In this study, we propose a new framework, Feature Enforcing Physics-Informed Neural Networks (FE-PINN), that can overcome the challenge of an imbalanced loss function in vanilla PINN. This

imbalance in the loss function can hinder the convergence of the neural network and require loss weighting in the objective function and consequently needs the time-consuming process of hyperparameter tuning. To avoid this issue, our framework uses a process called “smart initialization” to create a new set of weights that already contain information about the boundary conditions of the problem. This is achieved by using a new clustered sampling approach and a new initial weights design for the neural network and training the neural network with the focus of learning only desired boundary conditions. As a result of this process, FE-PINN does not need loss weighting. We demonstrate the effectiveness of our framework on two benchmarks: 2D flow over a cylinder and an inverse problem with unknown inlet velocity. Our framework can be used as a fast and accurate tool for solving various PDEs across different fields.

2. Physics Informed Neural Network

Our study focuses on solving PDEs using a novel framework, which is a variation of the PINN approach. While Navier-Stokes equations have been the primary choice for addressing such problems in the majority of research studies in this field [27-29], the Cauchy-Euler equation was employed in this case to avoid the inclusion of a second-order derivative in the loss function. This is because calculating the second-order derivative for a neural network can be computationally expensive [45]. This challenge becomes even more noticeable when dealing with large neural networks, resulting in slower training time.

2.1 Loss Function and Training Challenges of Vanilla PINN

Similar to vanilla PINN, the standard form of the loss function is employed, which consists of two distinct components. One component corresponds to the boundary conditions, while the other component pertains to the PDE. The loss function is designed as follows:

$$\text{Loss Function} = L_{pde} + \lambda \times L_{boundary} \quad (1)$$

$$L_{pde} = f_0^2 + f_1^2 + f_2^2 + f_3^2 + f_4^2 + f_5^2 \quad (2)$$

$$f_0 = \frac{\partial u}{\partial x} + \frac{\partial v}{\partial y} \quad (3)$$

$$f_1 = \rho \left(u \times \frac{\partial u}{\partial x} + v \times \frac{\partial u}{\partial y} \right) - \frac{\partial \sigma_{xx}}{\partial x} - \frac{\partial \sigma_{xy}}{\partial y} \quad (4)$$

$$f_2 = \rho \left(u \times \frac{\partial v}{\partial x} + v \times \frac{\partial v}{\partial y} \right) - \frac{\partial \sigma_{xy}}{\partial x} - \frac{\partial \sigma_{yy}}{\partial y} \quad (5)$$

$$f_3 = -p + 2 \times \mu \times \frac{\partial u}{\partial x} - \sigma_{xx} \quad (6)$$

$$f_4 = -p + 2 \times \mu \times \frac{\partial v}{\partial y} - \sigma_{yy} \quad (7)$$

$$f_5 = \mu \left(\frac{\partial u}{\partial y} + \frac{\partial v}{\partial x} \right) - \sigma_{xy} \quad (8)$$

$$L_{boundary} = \|Predictions(x, y | w) - Labels\|^2 \quad (9)$$

Where ρ represents the fluid density, u and v denote the x and y components of the velocity vector, μ represents the dynamic viscosity, p corresponds to the fluid pressure, and σ denotes the stress. The loss function quantifies the difference between the predicted output of the neural network and the boundary value and uses PDE loss to understand the governing equation. During training, the weights of the neural network are updated iteratively to minimize the loss function. This iterative update allows for the calculation of the velocity and pressure field within the given domain. However, in some cases optimizing the loss function can be challenging. The loss function consists of two parts: the boundary loss and the PDE loss. The boundary loss measures how well the model matches the ground truth values of the boundary condition, while the PDE loss measures how well the model satisfies the derivative values that form the PDE equation. However, these two parts have different scales and magnitudes, which makes the loss function imbalanced and difficult to optimize. To address this issue, researchers have developed innovative strategies to modify the weighting factor, λ , that balances the two loss components in [Equation \(1\)](#) [30-32]. These studies aim to design adaptive weighting schemes and dynamic updates for λ to balance the loss function. However, it is crucial to acknowledge that achieving a balanced loss function through these methods may not be effective for different problems. Moreover, determining the optimal value for λ can be a time-consuming task. In this study, a novel approach is proposed to address the issue of balancing the loss function in neural networks. It is important to note that in this study, λ is set to 1 for all cases. Despite the introduced framework in this study setting $\lambda = 1$ for vanilla PINN can result in an imbalance between the terms of the loss function. The imbalance loss function can pose a significant challenge in the training of neural networks. Tuning the λ term in the loss function is a difficult task due to the influence of various random factors. One such factor is the ratio between the total number of domain and boundary points, which can affect the optimal value for λ . Vanilla PINN is trained using [Equation \(1\)](#) as the loss function to investigate this impact of λ on the convergence. Note that this neural network takes x and y as inputs and outputs u , v , p ,

σ_{xx} , σ_{xy} and σ_{yy} . Latin hypercube sampling (LHS) and random sampling method are used to select domain points and boundary points, respectively. [Figure 1](#) shows the distribution of the selected points. The density of selected points around the cylinder is higher than other parts of the domain to capture the underlying physics more accurately.

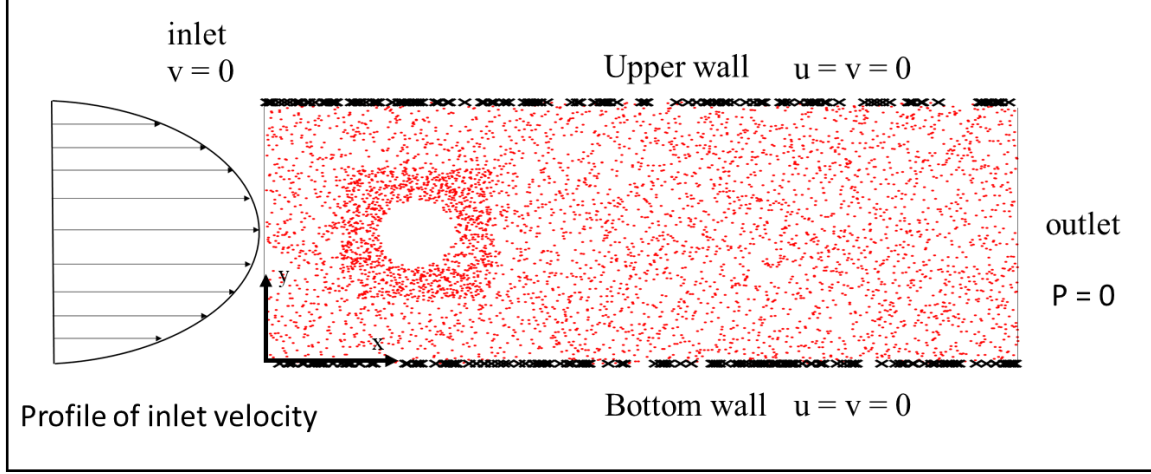


Figure 1: Selected points using LHS method and random sampling method

Tuning λ can be a difficult task due to the influence of various random factors. One such factor is the ratio of the number of domain to boundary points, which can affect the optimal value for λ . To illustrate this, two cases are considered that have a slight difference in the ratio of the number of the domain to boundary points. This ratio is considered as 0.035 for case 1 and 0.033 for case 2, respectively. To determine the optimal value of λ , the vanilla PINN is trained using the PyTorch LBFGS optimizer. [Table 1](#) shows how different ratios can affect the optimal value of λ . As shown in [Table 1](#), a slight change in the ratio of the number of domain to boundary points can result in a dramatic change in training time or divergence. For example, when the value of λ is 0.5, the training time is much faster in case 2, whereas the training time for $\lambda = 1$ is faster in case 1. Note that the training process is stopped when the loss value reaches a threshold of 10^{-3} .

Table 1: Training time, in minutes, for different λ to converge to a loss value of 10^{-3} in case 1 and case 2

	$\lambda = 0.1$	$\lambda = 0.5$	$\lambda = 1$	$\lambda = 1.1$	$\lambda = 1.5$	$\lambda = 5$
Case 1	Not Converged	40.883	17.900	15.283	25.050	14.266
Case 2	Not Converged	13.450	27.550	25.583	15.933	28.616

As can be seen in [Table 1](#), selecting the optimal value for the hyperparameter λ is crucial in saving time and resources. However, the process of tuning this hyperparameter can be both time-consuming and challenging. Choosing an incorrect value for λ can exacerbate the issue, resulting in a failure for the loss value to converge to the desired threshold. For instance, as shown in [Table 1](#), using a λ value of 0.1 failed to converge to the threshold. If the threshold is set at a lower value, such as 10^{-4} , the process becomes even more challenging and time-consuming, with an increased risk that the loss function may not converge to the desired threshold. [Figure 2](#) illustrates how the different λ values can affect the time of convergence and whether convergence is possible for the set threshold. As shown in [Figure 2](#), using a value of $\lambda = 1$ makes it impossible to converge to a threshold of 10^{-4} .

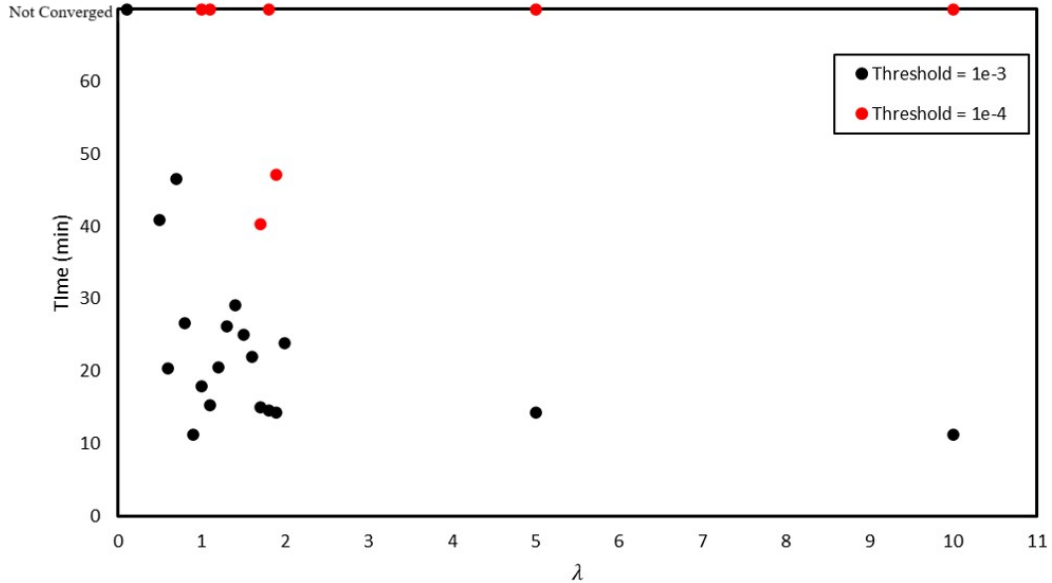


Figure 2: Illustration of how tuning λ can impact the ability to reach different thresholds of 10^{-3} and 10^{-4} for a constant ratio of domain point to boundary point.

3. Feature Enforcing Framework

The neural network is defined by its layers and neurons. These layers are responsible for learning more and more complex features as they move deeper into the network. In practice, the initial layers of a multi-layer perceptron (MLP) struggle to capture high-frequency details, including low-level details (in this case, the main underlying physics of the problem), during their learning. Addressing this issue requires the incorporation of additional techniques to rectify the situation [\[33\]](#). The mentioned fact inspires us to create the following FE-framework. To effectively teach the overall pattern to the first layers of the MLP, we employ the following process:

1. **Smart Initialization:** Initially, we generate new weights by forcing the neural network to learn the underlying physics of the problem. This includes understanding the overall physics of the problem with a low-cost training process. This step is referred to as "smart initialization" and the new set of weights is called "smart weights".
2. **Increasing Model Complexity and Training:** During this stage, a new neural network is created by utilizing the smart initialization method. Furthermore, extra layers are added to refine the calculation made during the smart initialization process. Subsequently, we train the neural network using a loss function that encompasses all boundary condition terms along the PDE loss term despite the previous process.

3.1 Smart Initialization

Smart initialization is a process that produces the smart weights for a model, which has an understanding of the underlying physics features. This is achieved through a low-cost training process that learns the boundary conditions in different parts of the domain. The goal of smart initialization is to improve the convergence of PINNs, rather than achieving a high level of success in predicting the main solution of the problem. This approach is similar to the pretext task in self-supervised learning, where the model is forced to learn good features about images by performing tasks such as predicting rotation. As a result, the model can perform better on the target task, even if it cannot predict rotation for all inputs [46]. The smart weights also make the training process of vanilla PINN smoother. One of the benefits of this approach is that it eliminates the need for time-consuming and often unreliable hyperparameter tuning, which can significantly slow down the training process. This is because the smart weights already have an understanding of boundary conditions.

3.1.1 Introducing a Clustered Sampling Approach

The method searches for any potential obstacles that may impede fluid flow, such as a 2D cylinder in this case. If an obstacle is present, the method encloses it with a surrounding square to account for its presence (step 1 of [Figure 3](#)). The distance between the square's sides and the domain's boundaries is calculated based on how far apart the square's x and y maximum and minimum values are from the domain's boundaries, respectively. Based on the complexity of the geometry, the domain is divided into a desired number of subdomains. In this case, there are ten

subdomains plus the first square. The sides of the subdomains are equally spaced from the left, right, top, and bottom sides of each subdomain (step 2 of [Figure 3](#)). Each subdomain is shown with a different color in [Figure 3](#). The LHS method is utilized in each subdomain separately to produce points. n different neural networks (in this case $n = 10$) are initialized with the Xavier scheme. Each of these neural networks takes x and y coordinates of these selected points as inputs and outputs the values of u , v , p , σ_{xx} , σ_{xy} and σ_{yy} . The neural network uses only [Equation \(2\)](#) as its loss function, which measures the PDE score of each point. Selected points from each subdomain are used as inputs for these neural networks (step 3 of [Figure 3](#)). After the forward pass in the neural network, the PDE score of each individual point is calculated by applying [Equation \(2\)](#) to the predicted values. It is worth noting that the PDE score is assigned to each point by calculating [Equation \(2\)](#) for the specific location of that point (x,y) but PDE loss is the averaged-out value of PDE scores (It is one of the loss terms of vanilla PINN's loss function). Note that the process of initializing neural networks is stochastic, which means that the calculated PDE scores may vary for the individual point depending on the state of the initial weights. This implies that different neural networks may assign different PDE scores to individual points in the domain. This is the reason behind utilizing n -different neural networks. Points in each subdomain are used as inputs for just one forward pass of these neural networks to calculate the PDE score, resulting in n different scores for each point. Then, the top 10 percent of points with the highest PDE scores are selected for each neural network in each subdomain. Due to the stochastic nature of this process, there is a chance that a point may be selected more than once by two different neural networks out of n . Before the training process, any duplicate points will be deleted. The final set of points that are chosen serves as a clustered point representation of the domain, capturing random points with high PDE scores (step 4 of [Figure 3](#)). Note that repeating this process results in different point configurations in step 4. One of these configurations is shown as a sample in [Figure 3](#).

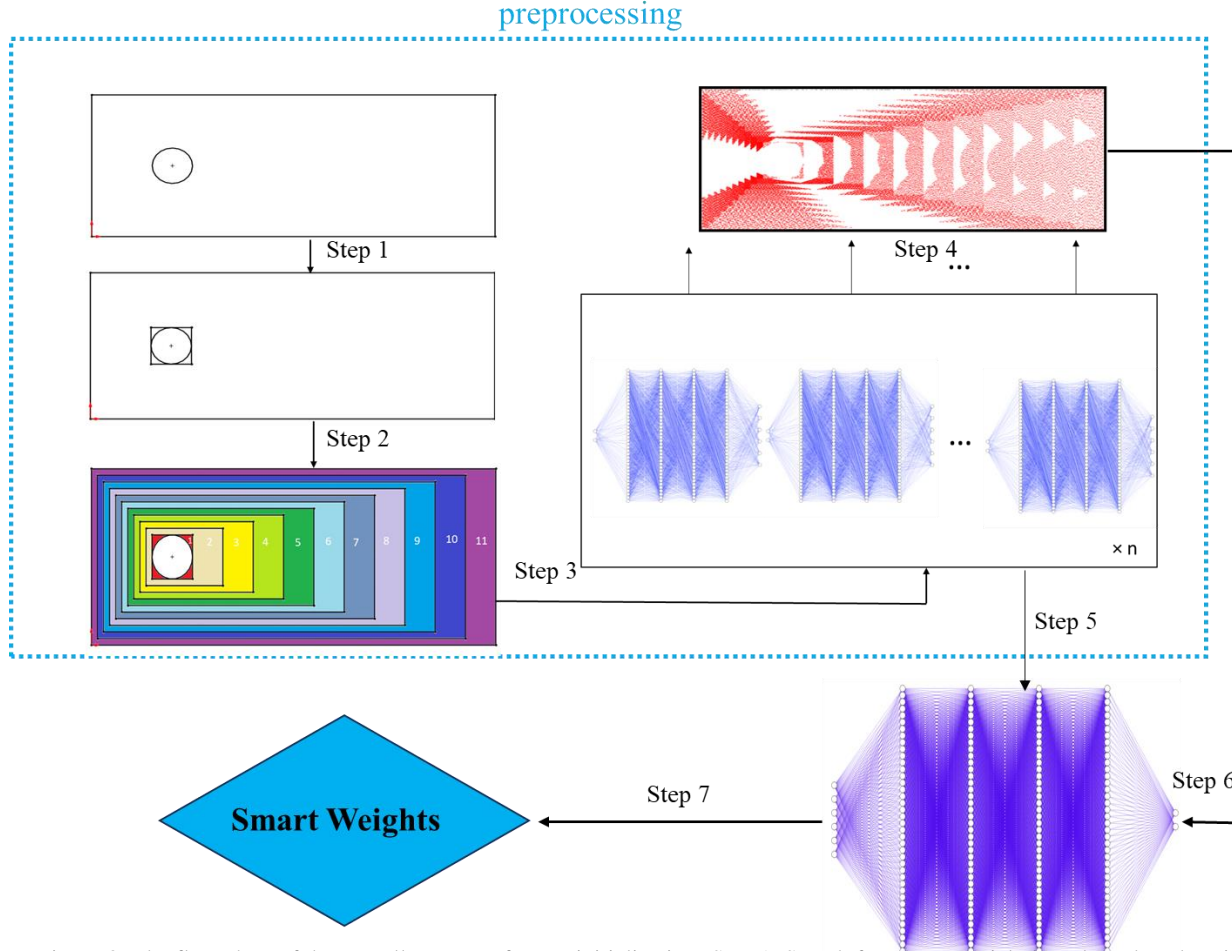


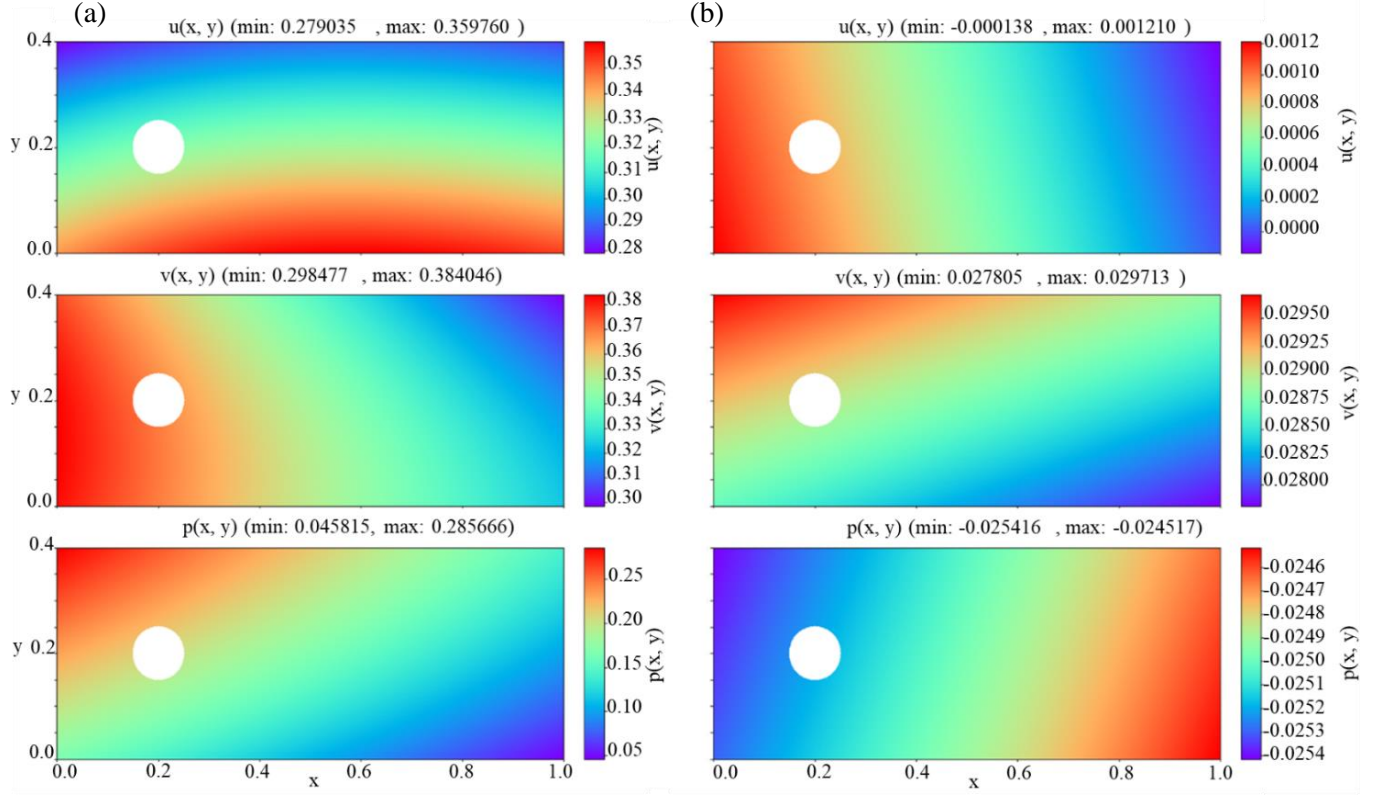
Figure 3: The flow chart of the overall process of smart initialization. Step 1: Search for any potential obstacle and enclose it. Step 2: Divide the domain into subdomains. Step 3: Employ LHS in each subdomain to create points then use each subdomain for the forward pass of each neural network. Step 4: Calculate the PDE score for each subdomain with each neural network and hold points with the highest score. Step 5: Create untrained averaged-out neural network. Step 6: Use clustered domain points as input. Step 7: Train the neural network to create Foundation Network.

In the last step of the preprocessing, the weights and biases of these n -utilized neural networks are averaged out to create a new neural network called the untrained averaged-out neural network (step 5 of [Figure 3](#)). In [Figure 4](#), a comparison is made between the outputs and the derivatives of the outputs with respect to the inputs of the untrained averaged-out neural network and a neural network initialized with the Xavier scheme. As shown in the first row of [Figures 4\(a & b\)](#), the value of u for the untrained averaged-out neural network is close to zero, with a small change of 0.001348 (first row of [Figure 4\(a\)](#)). However, the value of u for the neural network initialized with the Xavier scheme varies, with a difference of 0.080725 between the maximum and minimum values (first row of [Figure 4\(b\)](#)). This difference is of a much greater order of magnitude than the

change in the output of the untrained averaged-out neural network. This pattern is also observed for other outputs, as shown in the second and third rows of [Figures 4 \(a & b\)](#) for the values of v and p , respectively. [Figures 4\(c & d\)](#) show that the derivative values ($\frac{\partial u}{\partial x}$ is used as an example to show this issue) of the averaged-out neural network are much smaller order of magnitude than that of the neural network initialized with the Xavier scheme. This means that the values of u , v , and p vary smoothly in the whole domain. For instance, by looking at the second row of [Figures 4\(c & d\)](#), it indicates that the range of variation is 0.001228 for the untrained averaged-out neural network, while for the network initialized with Xavier, the range of variation is 0.0933043 across the domain for the $\frac{\partial u}{\partial x}$ value. We repeated the process, and the results are shown in the second and third rows of [Figure 4 \(c & d\)](#). They demonstrate that the range of variation of $\frac{\partial u}{\partial x}$ for the untrained averaged-out neural network is still much smaller than that of the neural network initialized with the Xavier scheme, regardless of the randomness involved in the procedure. Hence the untrained averaged-out neural network systematically calculates derivatives lower than a neural network initialized with the Xavier scheme. In [Table 2](#), the value of PDE loss is calculated for both the untrained averaged-out neural network and a neural network initialized with the Xavier scheme. As shown in [Table 2](#), the untrained averaged-out neural network assigns a lower PDE loss value to domain points because the derivatives calculated by the model are smaller than those calculated by a neural network initialized with the Xavier scheme. This is because of the fact that PDE is formed by partial derivatives of outputs. The procedure is repeated four times for different random seeds and is shown in the first four rows of [Table 2](#). It demonstrates that the PDE loss of the untrained averaged-out neural network is orders of magnitude smaller than a neural network initialized with the Xavier scheme for all rows. Therefore, the procedure is repeatable for different random seeds and is not based on randomness. Note that in the first four rows of [Table 2](#), the domain points are the same, but different random seeds are used for generating the two neural networks. Row 5 confirms its validity for the smaller number of domain points.

Table 2: Calculated PDE loss for the untrained averaged-out neural network and a neural network initialized with Xavier scheme

	Total domain points	Random neural network PDE loss	Untrained averaged out neural network PDE loss
Case 1 (random seed #1)	371760	1.2691	0.0034
Case 1 (random seed #2)	371760	1.4661	0.0049
Case 1 (random seed #3)	371760	0.9479	0.0007
Case 1 (random seed #4)	371760	0.5480	0.0043
Case 2	47297	0.5199	0.0011



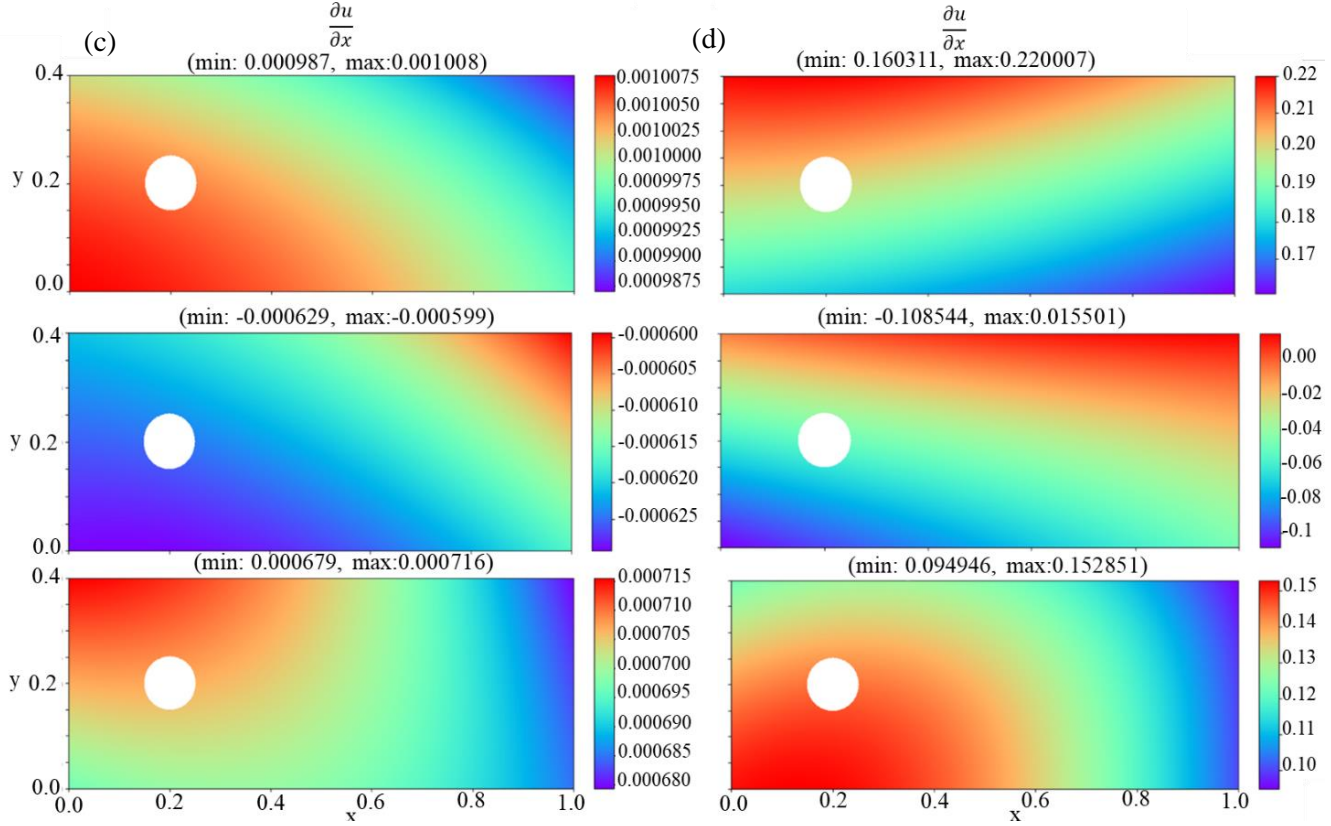


Figure 4: For better visualization, domain points are selected using the LHS method. The first three figures display (u, v, p) , for the untrained averaged-out neural network and a neural network initialized using Xavier scheme (a, b). The last three figures display value of du/dx for untrained averaged-out neural network and a neural network initialized using Xavier scheme for three different random states (c, d).

3.1.2 Preparing smart weights using FE-Framework Details

The FE-framework is designed to prioritize learning the overall patterns with the first layers of the neural network. With this in mind, the neural network's architecture is carefully crafted. The averaged-out neural network is at last trained with the loss function containing PDE loss and the no-slip boundary condition on side walls with clustered domain points as input (loss function = no-slip boundary condition on side walls + PDE loss). The trained version of this neural network is called Foundation Network 1 and is developed with 4 hidden layers and 40 neurons in each layer. This neural network takes x and y as inputs and outputs $u, v, p, \sigma_{xx}, \sigma_{xy},$ and σ_{yy} . The training process is carried out using the ADAM optimizer with a learning rate of 3×10^{-4} , on the

clustered domain points (step 7 of [Figure 3](#)). Note that in this step, the loss function does not have any term related to the inlet velocity, boundary condition on the cylinder, and outlet pressure. The training process finishes quickly because the starting point is near a local minimum point or a saddle point. During the training procedure, the neural network learns the no-slip boundary conditions on the side walls because of the simplicity of this pattern. However, the PDE terms cannot converge to zero and the process converges to the nearest local minimum. It is worth noting that if the preprocessing (step 1 to step 6 in [Figure 3](#)) is not considered and training in step 7 is done with LHS domain points and a neural network initialized with the Xavier scheme, the neural network would predict trivial solution (prediction u and v equal to zero in the entire domain). In fact, the preprocessing considered in this study prevents the neural network from predicting u and v equal to zero in the entire domain and neutralizes the effect of the absence of the other boundary conditions on convergence. Thus, the preprocessing leads to the initiation of the optimization process within the vicinity of a saddle point or local minimum. Adaptive optimizers like ADAM face difficulties in converging to the global minimum when starting from a saddle point or local minimum. One potential reason for this is that outputs are not sensitive to input changes across the whole domain. In other words, the variation of u , v , and p obtained by the untrained averaged-out neural network is orders of magnitude smaller than those of the neural network initialized by the Xavier scheme as shown in [Figure 4](#) and [Table 2](#). This behavior demonstrates that this approach can selectively learn the no-slip boundary condition on side walls. This fact is used to force the neural network to only learn the desired features. In other words, the focus shifts from converging to the solution of the governing equation on the domain to forcing the untrained averaged-out neural network to learn the no-slip boundary conditions. This is similar to predicting rotation in self-supervised learning [46]. Even if the Foundation Network cannot completely predict no-slip boundary conditions at the end of the training, it will still make the vanilla PINN's training loop smoother.

While the previous changes are adequate, if more information about the domain is available, it can be used to speed up the framework. It is recommended to use specific characteristics of the underlying physics being modeled in the loss function. For instance, the inlet velocity profile can vary based on the application. By incorporating these features into the loss function, the resulting model is better equipped to capture the relevant physical behavior of the fluid flow. In the case of flow over the 2D cylinder, if the inlet velocity profile is parabolic, then it is utilized in the loss

function as an additional boundary condition term to enhance the acceleration of the framework (loss function = no-slip boundary condition on side walls + inlet velocity boundary condition + PDE loss). This implementation assumes a fully developed flow at the inlet of the domain, with a zero y-component of velocity. The trained version of this neural network is called Foundation Network 2. The only difference between Foundation Network 2 and Foundation Network 1 is the addition of a new loss term to the loss function, which takes into account the inlet velocity profile. The training process allows the Foundation Networks to predict the values of u , v , and p , as shown in [Figure 5](#). At the end of training smart weights are produced (in step 7 of [Figure 3](#)). Note that the training process for Foundation Network 1 takes 0.3 minutes on average, while that for Foundation Network 2 requires 1.2 minutes on average with GPU RTX 4080. It is important to note that for better visualization in [Figure 5](#), the trained Foundation Networks are fed with a complete set of domain points especially the points around the cylinder.

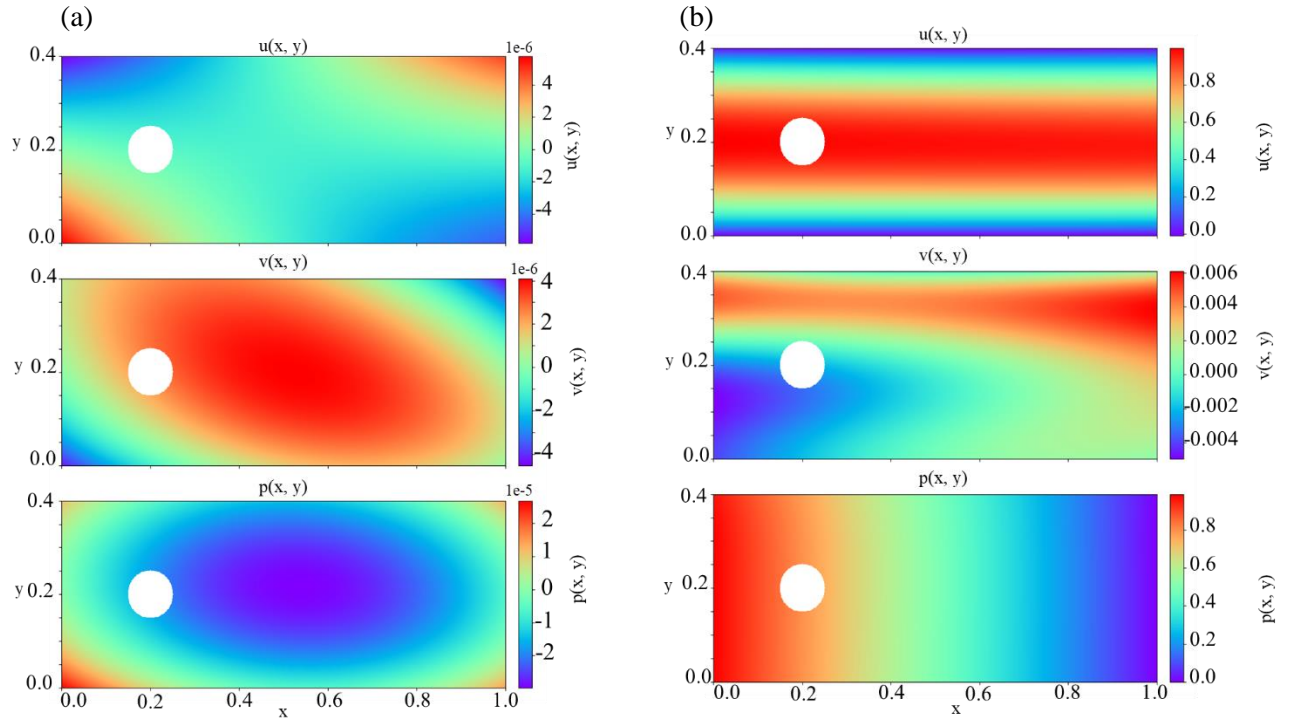


Figure 5: outputs of (a) Foundation Network 1, and (b) Foundation Network 2.

3.2 Increasing Model Complexity and Training

The training process begins by increasing the Foundation Networks complexity by adding more layers on top of them before the output layer. The blue layers in [Figure 6](#) show the smart

weights for Foundation Networks, while the red ones are the newly added layers that are initialized with the Xavier scheme to increase the neural network capacity. The next step involves training the newly created model called FE-PINN to improve the accuracy of its predictions. In the training process, the same approach as vanilla PINN is used, with λ being kept at 1 for the entire training process. The loss function contains PDE loss and all boundary conditions ([Equation \(1\)](#)). Domain points are selected using the LHS method, as illustrated in [Figure 1](#). The Torch library's LBFGS method is used for the optimization process, with the default configuration with a minor modification; the model's weight matrix is flattened into a 1D tensor and unflatten back to the original shape during each training step. The reason for flattening and unflattening the weight matrix is to allow the LBFGS optimizer to work on a 1D tensor of the weight matrix instead of the original multi-dimensional tensor. This can simplify the optimization process and make it easier for the optimizer to find an optimal solution. [Algorithm 1](#) presents a step-by-step guide for implementing FE-PINN.

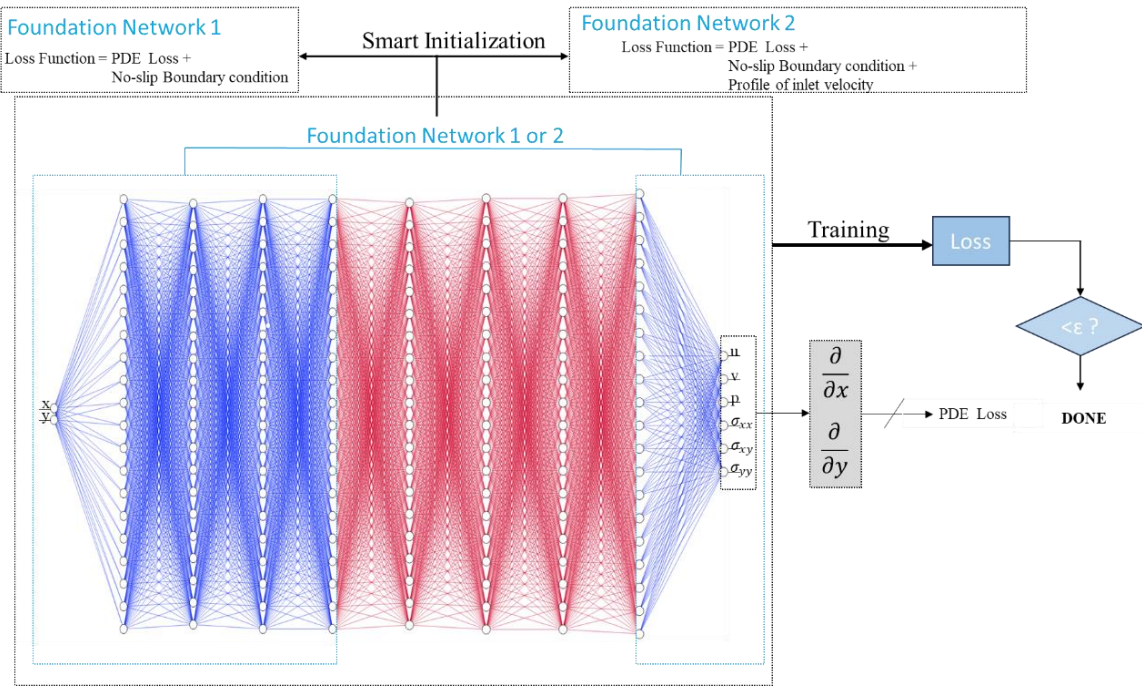


Figure 6: A schematic of FE-PINN

Algorithm 1: The step-by-step process of FE-PINN.	
1.	Smart Initialization
1.1	Identify any obstacle in the domain and enclose it.

1.2	Divide the domain into the desired number of subdomains according to the geometry.
1.3	Employ the LHS method in each subdomain.
1.4	For n steps, calculate the PDE score using a neural network for each point in each subdomain and select 10 percent of the points with the highest PDE score in each step. # n is the number of the total employed neural networks.
1.4	Drop any duplicate points. # Clustered points are generated in this step.
1.5	Average out the weights and biases of all n neural networks to create untrained averaged-out neural network.
1.6	Train the step 1.5 model on the selected points in step 1.4 by using a loss function that incorporates the no-slip boundary condition with PDE loss. If possible, use boundary knowledge to improve the loss function. # Creating Foundation Network
2.	Increasing Model Complexity and Training
2.1	Add new hidden layers before the output layer of the Foundation Network in step 1.6.
2.2	Train the FE-PINN on the entire domain points by using a loss function that considers PDE loss and all boundary conditions.

4. Results and Discussion

4.1 2D Flow around cylinder

The FE-PINN is a highly efficient solution that eliminates the need for the time-consuming process of λ tuning with Smart Initialization taking only about one minute. [Table 3](#) shows that, on average, the FE-PINN Smart Initialization and training times are faster compared to the vanilla PINN hyperparameter tuning and training times, respectively. We use random search to quantify the average time required to find the optimal λ value for vanilla PINN. This process is repeated five times to make the total time independent from randomness. For each time, the tuning time and the convergence time of the best λ value are measured. Then, the average times are calculated and reported in [Table 3](#). This [table](#) shows that on average, the FE-PINN Smart Initialization process is 574 times faster than λ tuning in vanilla PINN when using Foundation Network 1, and 144 times faster when using Foundation Network 2. Even with the optimal λ value, FE-PINN outperforms vanilla PINN by speeding up the average training time by 1.98 times for Foundation Network 1 and by 2.2 times for Foundation Network 2. This demonstrates that FE-PINN not only eliminates the need for hyperparameter tuning but also trains faster on the target task.

Table 3: Time on average, in minutes, required for tuning time, smart initialization and training time for vanilla PINN and Foundation Networks.

	Vanilla PINN	Foundation Network 1	Foundation Network 2
Average Tuning time	172.3	----	----
Smart Initialization	----	0.3	1.2
Average training time	47.4	23.9	21.4
Total time for reaching 10^{-4}	219.6	24.2	22.6

The big O notation is used to describe the growth rate of the number of operations, ignoring constant factors and lower-order terms. The big O (time complexity) of training a PINN depends on various factors such as the total number of layers, the total number of neurons per layer, the number of inputs and output features, the number of domain points, the number of epochs, calculated derivatives, the optimization algorithm and, tuning λ value. In this study, both FE-PINN and vanilla PINN have the exact same characteristics, with one difference: the λ value in vanilla PINN needs to be tuned, but FE-PINN replaced this process with a low-cost, smart initialization process. The difference between the big O notation for FE-PINN and vanilla PINN lies in the need to explore the best value for λ in the loss function of vanilla PINN. For vanilla PINN, in the best-case scenario, the first selected λ value converges to the desired threshold ($O(1)$), while in the worst-case scenario, all possible values must be explored ($O(n)$), where n is the number of iterations performed to find the best value of λ . However, in the case of FE-PINN, there is no need for such a process. Instead, a low-cost smart initialization can replace exploring different λ values, with an average training time of just one minute. It is important to note that for FE-PINN, the time complexity is $O(1)$, which means it is constant and does not depend on finding the best λ value. [Figure 7](#) offers a straightforward depiction of how Foundation Network 2's loss function smoothly reaches its global minimum. This highlights the success of the training process in optimizing the loss function and accomplishing the desired outcome. In [Figure 8](#) the outputs of vanilla PINN and FE-PINN are compared visually.

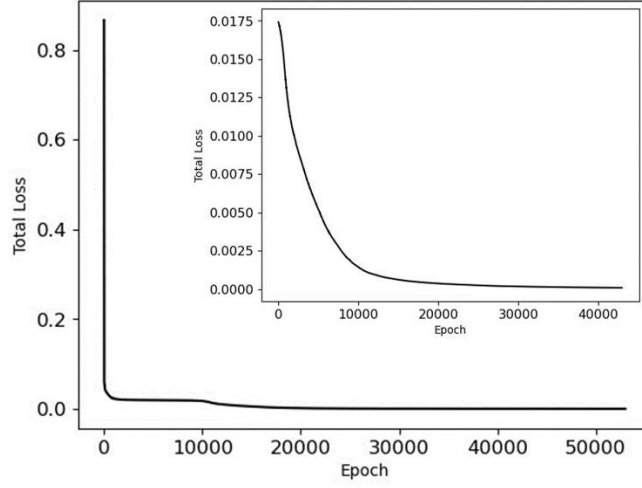


Figure 7 illustration of how the neural network loss value changes versus Epoch.

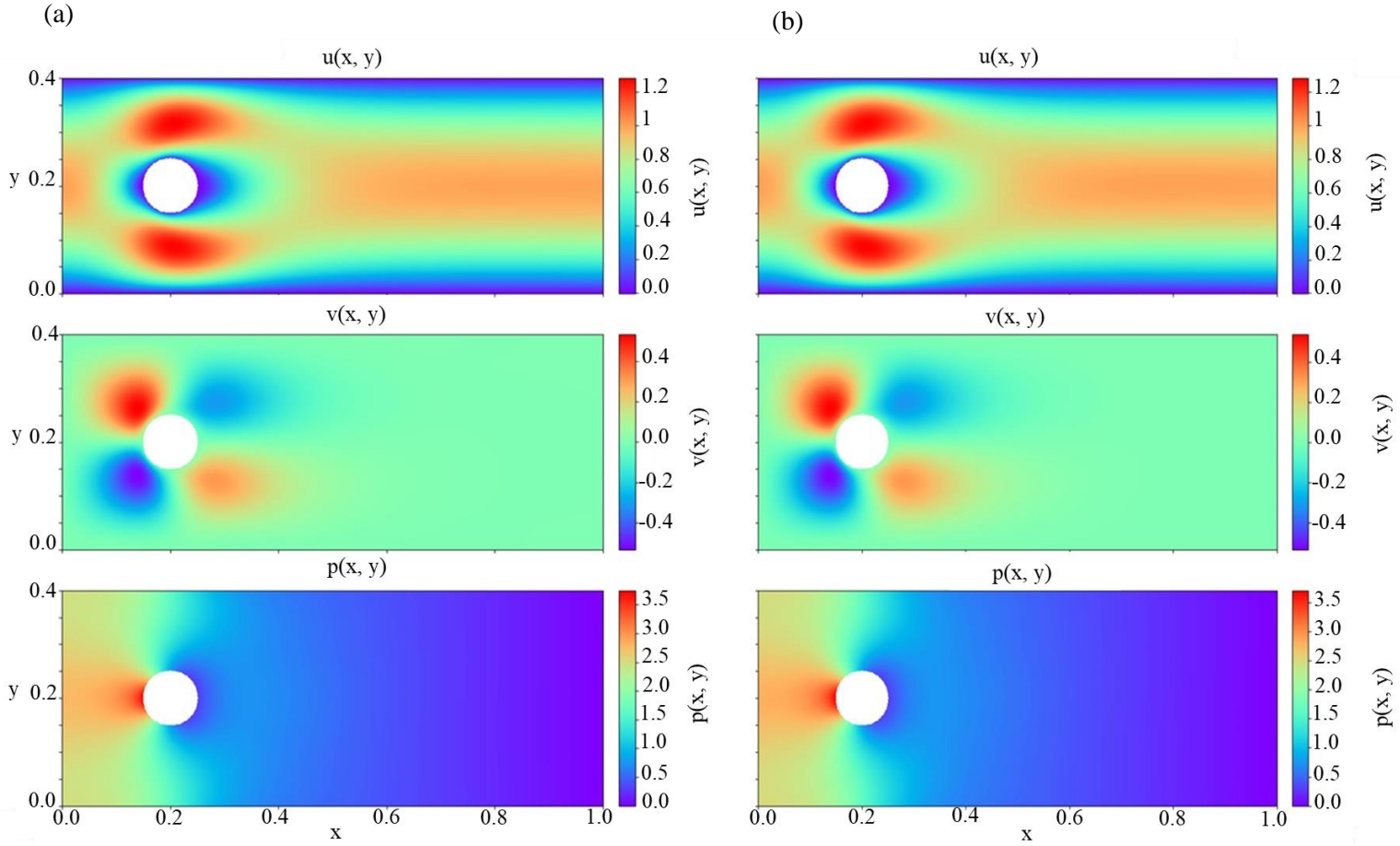


Figure 8: A comparison is made between the (u,v,p) predicted by (a) FE-PINN and (b) vanilla PINN for the flow over a 2D cylinder.

4.2 Inverse Problem

Vanilla PINN is a promising tool for solving inverse problems, which are ill-posed because of unknown boundary conditions. In this section, we compare the performance of FE-PINN and vanilla PINN in solving an inverse problem with the following characteristics: the inlet velocity is unknown, the outlet pressure is zero, and the no-slip boundary condition is applied to the side walls (the boundary conditions are shown in [Figure 9](#)). Moreover, we have 60 domain points with known u and v values, as indicated by the blue marks in [Figure 9](#). As demonstrated in the previous section, FE-PINN offers several advantages over vanilla PINN. Not only it eliminates the need of λ value tuning, but it also achieves faster convergence, even when the optimal λ value for vanilla PINN is known. In order to solve the inverse problem using the FE-PINN method, we employ Foundation Network 2. Since the inlet velocity is unknown, u and v values of 60 domain points are used to improve the loss function in step 1.6 of the [Algorithm 1](#). At this step the Loss function is equal to the summation of no-slip boundary condition on side walls, $L_{Inverse\ problem}$, and PDE loss

$$L_{Inverse\ problem} = \frac{1}{n} \sum_{i=0}^n \|Predictions(x, y | w) - u(x, y)\|^2 + \|Predictions(x, y | w) - v(x, y)\|^2, n = 60 \quad (10)$$

Once the training is completed with the mentioned loss function, the smart weights will be ready for use.

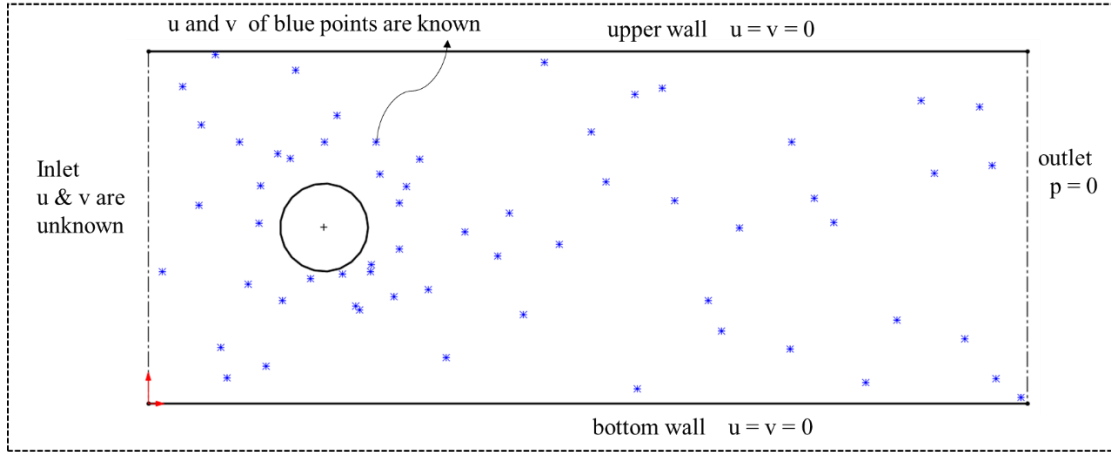


Figure 9: Inverse Problem of finding inlet velocity.

To ensure a fair comparison, both the FE-PINN and vanilla PINN are trained under similar conditions. This includes using the same learning rate, optimization algorithm (LBFGS), the same number of domain and boundary points, and the same structure. Note that the structure of both the

vanilla PINN and FE-PINN remains consistent with the previous section, including the same number of layers, inputs, and neurons (Loss function = no-slip boundary condition on side walls and cylinder + $L_{Inverse\ problem}$ + PDE loss + outlet boundary condition). The training phase is stopped when the loss value reaches a threshold of 10^{-4} , which is set for both neural networks. [Table 4](#) compares the average training time of FE-PINN and vanilla PINN. To make the total time independent from randomness, FE-PINN is trained three different times. The other columns of [Table 4](#) show the training time for vanilla PINN with different λ values. The last row of [Table 4](#) uses the R-squared metric to compare how well these models can predict the inlet velocity.

Table 4: Displaying the time, in minutes, required to converge to total loss value of 10^{-4} .

	$\lambda = 1$	$\lambda = 1.3$	$\lambda = 1.5$	Foundation Network 2 #1	Foundation Network 2 #2	Foundation Network 2 #3
Smart Initialization	-----	-----	-----	0.99	1.2	1.3
Training Time	24.65	27.86	35.40	12.99	13.11	13.61
Accuracy	0.9980	0.9975	0.9960	0.9983	0.9983	0.9980

[Table 4](#) shows that FE-PINN is approximately twice as fast as vanilla PINN in this benchmark, without any need for tuning λ . Tuning the λ value can make the convergence for vanilla PINN faster. Note that in the case of the inverse problem in this study, most of the λ values for vanilla PINN can reach the threshold of 10^{-4} , except for a few. For instance, a λ value of 1.2 converges to 0.0001047 loss value in 35.42 minutes and can't reach lower loss values. For this problem, the main benefit of choosing the optimal λ value is speeding up the training process. As seen in [Table 3](#) and [Table 4](#), FE-PINN still converges faster to the desired threshold even with tuning λ for vanilla PINN.

5. Conclusion

In this study, we propose a new data-free framework, Feature Enforcing-Physics Informed Neural Networks (FE-PINN), to overcome the challenge of an imbalanced loss function in vanilla PINN. Unlike Computational Fluid Dynamics (CFD) methods, vanilla PINN is mesh-free, generalizable, and more suitable for inverse problems. However, it struggles to converge due to the imbalanced loss function. A common solution is loss weighting, but the need for hyperparameter tuning is time-consuming. FE-PINN avoids loss weighting and converges faster to the fixed threshold. It does so by using a process called "smart initialization", which generates

new weights that enforce the neural network to learn the underlying physics of the problem. To this end, clustered points are selected and then smart weights are obtained for a Foundation network with clustered points as inputs. Next, extra layers are added to refine the calculation made during the smart initialization process and the neural network is trained using a loss function that encompasses all boundary condition terms and PDE loss. For 2D flow over a cylinder as a benchmark, the Foundation network 1 is considered in which the loss function is the summation of PDE loss and no-slip boundary condition on the side walls, while the Foundation network 2 is the summation of PDE loss and no-slip boundary condition and inlet velocity. As a result, smart initialization in FE-PINN for Foundation networks 1 and 2 are 574 and 144 times faster than hyperparameter tuning in vanilla PINN. Even with the optimal loss weight value, FE-PINN outperforms vanilla PINN by speeding up the average training time by 1.98 and 2 times for Foundation Networks 1 and 2. Also, the ability of the proposed approach is shown for an inverse problem. To find the inlet velocity for a 2D flow over a cylinder with 60 points in the domain with known u and v , FE-PINN is twice faster than vanilla PINN with the knowledge of optimal weight loss value for vanilla PINN. FE-PINN is a promising approach for solving different forms of PDEs and can be used in more complex problems. This method could be applied to more complex architecture for more complicated problems.

Author Contributions: Mahyar Jahaninasab; Methodology & writing Mohamad Ali Bijarchi; review & editing

Funding: This research received no external funding.

Code Availability Statement: The code will be published at <https://github.com/mahyar-jahaninasab/Feature-Enforcing-PINN>

Conflicts of Interest: The authors declare no conflict of interest.

Acknowledgment: The authors would like to acknowledge Miss. Mina Rezaie & Mr. Ehsan Ghaderi for their helpful and kind support.

References

- [1] Raissi, Maziar, Paris Perdikaris, and George E. Karniadakis. "Physics-informed neural networks: A deep learning framework for solving forward and inverse problems involving nonlinear partial differential equations." *Journal of Computational physics* 378 (2019): 686-707.
- [2] Bai, Yuexing, Temuer Chaolu, and Suda Bilige. "The application of improved physics-informed neural network (IPINN) method in finance." *Nonlinear Dynamics* 107, no. 4 (2022): 3655-3667.
- [3] Cai, Shengze, Zhicheng Wang, Sifan Wang, Paris Perdikaris, and George Em Karniadakis. "Physics-informed neural networks for heat transfer problems." *Journal of Heat Transfer* 143, no. 6 (2021): 060801
- [4] Bararnia, Hassan, and Mehdi Esmaeilpour. "On the application of physics informed neural networks (PINN) to solve boundary layer thermal-fluid problems." *International Communications in Heat and Mass Transfer* 132 (2022): 105890.
- [5] Brunton, Steven L., Bernd R. Noack, and Petros Koumoutsakos. "Machine learning for fluid mechanics." *Annual review of fluid mechanics* 52 (2020): 477-508.
- [6] Jahaninasab, Mahyar, Ehsan Taheran, S. Alireza Zarabadi, Mohammadreza Aghaei, and Ali Rajabpour. 2023. "A Novel Approach for Reducing Feature Space Dimensionality and Developing a Universal Machine Learning Model for Coated Tubes in Cross-Flow Heat Exchangers" *Energies* 16, no. 13: 5185.
- [7] Kochkov, Dmitrii, Jamie A. Smith, Ayya Alieva, Qing Wang, Michael P. Brenner, and Stephan Hoyer. "Machine learning–accelerated computational fluid dynamics." *Proceedings of the National Academy of Sciences* 118, no. 21 (2021): e2101784118.
- [8] Kwon, Beomjin, Faizan Ejaz, and Leslie K. Hwang. "Machine learning for heat transfer correlations." *International Communications in Heat and Mass Transfer* 116 (2020): 104694.
- [9] Haghighat, Ehsan, Maziar Raissi, Adrian Moure, Hector Gomez, and Ruben Juanes. "A physics-informed deep learning framework for inversion and surrogate modeling in solid mechanics." *Computer Methods in Applied Mechanics and Engineering* 379 (2021): 113741.
- [10] Uddin, Ziya, Sai Ganga, Rishi Asthana, and Wubshet Ibrahim. "Wavelets based physics informed neural networks to solve non-linear differential equations." *Scientific Reports* 13, no. 1 (2023): 2882.
- [11] Chiu, Pao-Hsiung, Jian Cheng Wong, Chinchun Ooi, My Ha Dao, and Yew-Soon Ong. "CAN-PINN: A fast physics-informed neural network based on coupled-automatic–numerical differentiation method." *Computer Methods in Applied Mechanics and Engineering* 395 (2022): 114909.,
- [12] Wu, Chenxi, Min Zhu, Qinyang Tan, Yadhu Kartha, and Lu Lu. "A comprehensive study of non-adaptive and residual-based adaptive sampling for physics-informed neural networks." *Computer Methods in Applied Mechanics and Engineering* 403 (2023): 115671.

- [13] Bai, Jinshuai, Timon Rabczuk, Ashish Gupta, Laith Alzubaidi, and Yuantong Gu. "A physics-informed neural network technique based on a modified loss function for computational 2D and 3D solid mechanics." *Computational Mechanics* 71, no. 3 (2023): 543-562.
- [14] Kopaničáková, Alena, Hardik Kothari, George Em Karniadakis, and Rolf Krause. "Enhancing training of physics-informed neural networks using domain-decomposition based preconditioning strategies." *arXiv preprint arXiv:2306.17648* (2023).
- [15] Chronopoulou, Alexandra, Christos Baziotis, and Alexandros Potamianos. "An embarrassingly simple approach for transfer learning from pretrained language models." *arXiv preprint arXiv:1902.10547* (2019).
- [16] Ying, Wei, Yu Zhang, Junzhou Huang, and Qiang Yang. "Transfer learning via learning to transfer." In *International Conference on Machine Learning*, pp. 5085-5094. PMLR, 2018.
- [17] Cao, Bin, Sinno Jialin Pan, Yu Zhang, Dit-Yan Yeung, and Qiang Yang. "Adaptive transfer learning." In *proceedings of the AAAI Conference on Artificial Intelligence*, vol. 24, no. 1, pp. 407-412. 2010.
- [18] Shi, Nuobei, Qin Zeng, and Raymond Lee. "Language Chatbot–The Design and Implementation of English Language Transfer Learning Agent Apps." In *2020 IEEE 3rd International Conference on Automation, Electronics and Electrical Engineering (AUTEEE)*, pp. 403-407. IEEE, 2020.
- [19] Lin, Jianzhe, Liang Zhao, Qi Wang, Rabab Ward, and Z. Jane Wang. "DT-LET: Deep transfer learning by exploring where to transfer." *Neurocomputing* 390 (2020): 99-107.
- [20] Liu, Yang, Wen Liu, Xunshi Yan, Shuaiqi Guo, and Chen-an Zhang. "Adaptive transfer learning for PINN." *Journal of Computational Physics* (2023): 112291.
- [21] Chen, Xinhai, Chunye Gong, Qian Wan, Liang Deng, Yunbo Wan, Yang Liu, Bo Chen, and Jie Liu. "Transfer learning for deep neural network-based partial differential equations solving." *Advances in Aerodynamics* 3, no. 1 (2021): 1-14.
- [22] Goswami, Somdatta, Cosmin Anitescu, Souvik Chakraborty, and Timon Rabczuk. "Transfer learning enhanced physics informed neural network for phase-field modeling of fracture." *Theoretical and Applied Fracture Mechanics* 106 (2020): 102447..
- [23] Shi, Zhouxing, Yihan Wang, Huan Zhang, Jinfeng Yi, and Cho-Jui Hsieh. "Fast certified robust training with short warmup." *Advances in Neural Information Processing Systems* 34 (2021): 18335-18349.
- [24] Inda, Adan J. Garcia, Shao Y. Huang, Nevrez Immamoglu, and Wenwei Yu. "Physics informed neural network (PINN) for noise-robust phase-based magnetic resonance electrical properties tomography." In *2022 3rd URSI Atlantic and Asia Pacific Radio Science Meeting (AT-AP-RASC)*, pp. 1-4. IEEE, 2022.

- [25] Yan, Junjun, Xinhai Chen, Zhichao Wang, Enqiang Zhou, and Jie Liu. "ST-PINN: A Self-Training Physics-Informed Neural Network for Partial Differential Equations." *arXiv preprint arXiv:2306.09389* (2023).
- [26] Penwarden, Michael, Ameya D. Jagtap, Shandian Zhe, George Em Karniadakis, and Robert M. Kirby. "A unified scalable framework for causal sweeping strategies for Physics-Informed Neural Networks (PINNs) and their temporal decompositions." *arXiv preprint arXiv:2302.14227* (2023).
- [27] Jin, Xiaowei, Shengze Cai, Hui Li, and George Em Karniadakis. "NSFnets (Navier-Stokes flow nets): Physics-informed neural networks for the incompressible Navier-Stokes equations." *Journal of Computational Physics* 426 (2021): 109951.
- [28] Ranade, Rishikesh, Chris Hill, and Jay Pathak. "DiscretizationNet: A machine-learning based solver for Navier–Stokes equations using finite volume discretization." *Computer Methods in Applied Mechanics and Engineering* 378 (2021): 113722.
- [29] Oldenburg, Jan, Finja Borowski, Alper Öner, Klaus-Peter Schmitz, and Michael Stiehm. "Geometry aware physics informed neural network surrogate for solving Navier–Stokes equation (GAPINN)." *Advanced Modeling and Simulation in Engineering Sciences* 9, no. 1 (2022): 8.
- [30] Hillebrecht, Birgit, and Benjamin Unger. "Certified machine learning: A posteriori error estimation for physics-informed neural networks." In *2022 International Joint Conference on Neural Networks (IJCNN)*, pp. 1-8. IEEE, 2022.
- [31] Wang, Sifan, Shyam Sankaran, and Paris Perdikaris. "Respecting causality is all you need for training physics-informed neural networks." *arXiv preprint arXiv:2203.07404* (2022).
- [32] Maddu, Suryanarayana, Dominik Sturm, Christian L. Müller, and Ivo F. Sbalzarini. "Inverse Dirichlet weighting enables reliable training of physics informed neural networks." *Machine Learning: Science and Technology* 3, no. 1 (2022): 015026.
- [33] Tancik, Matthew, Pratul Srinivasan, Ben Mildenhall, Sara Fridovich-Keil, Nithin Raghavan, Utkarsh Singhal, Ravi Ramamoorthi, Jonathan Barron, and Ren Ng. "Fourier features let networks learn high frequency functions in low dimensional domains." *Advances in Neural Information Processing Systems* 33 (2020): 7537-7547.
- [34] Lu, Lu, Xuhui Meng, Zhiping Mao, and George Em Karniadakis. "DeepXDE: A deep learning library for solving differential equations." *SIAM review* 63, no. 1 (2021): 208-228.
- [35] Nabian, Mohammad Amin, Rini Jasmine Gladstone, and Hadi Meidani. "Efficient training of physics-informed neural networks via importance sampling." *Computer-Aided Civil and Infrastructure Engineering* 36, no. 8 (2021): 962-977.

- [36] Gao, Wenhan, and Chunmei Wang. "Active learning based sampling for high-dimensional nonlinear partial differential equations." *Journal of Computational Physics* 475 (2023): 111848.
- [37] Tang, Kejun, Xiaoliang Wan, and Chao Yang. "DAS-PINNs: A deep adaptive sampling method for solving high-dimensional partial differential equations." *Journal of Computational Physics* 476 (2023): 111868.
- [38] Zeng, Shaojie, Zong Zhang, and Qingsong Zou. "Adaptive deep neural networks methods for high-dimensional partial differential equations." *Journal of Computational Physics* 463 (2022): 111232.
- [39] Hanna, John M., Jose V. Aguado, Sebastien Comas-Cardona, Ramzi Askri, and Domenico Borzacchiello. "Residual-based adaptivity for two-phase flow simulation in porous media using physics-informed neural networks." *Computer Methods in Applied Mechanics and Engineering* 396 (2022): 115100.
- [40] Yu, Jeremy, Lu Lu, Xuhui Meng, and George Em Karniadakis. "Gradient-enhanced physics-informed neural networks for forward and inverse PDE problems." *Computer Methods in Applied Mechanics and Engineering* 393 (2022): 114823.
- [41] van der Bos, Fedderik, and Bernard J. Geurts. "Computational error-analysis of a discontinuous Galerkin discretization applied to large-eddy simulation of homogeneous turbulence." *Computer methods in applied mechanics and engineering* 199, no. 13-16 (2010): 903-915.
- [42] Jagtap, Ameya D., Ehsan Kharazmi, and George Em Karniadakis. "Conservative physics-informed neural networks on discrete domains for conservation laws: Applications to forward and inverse problems." *Computer Methods in Applied Mechanics and Engineering* 365 (2020): 113028.
- [43] Haghighat, Ehsan, Danial Amini, and Ruben Juanes. "Physics-informed neural network simulation of multiphase poroelasticity using stress-split sequential training." *Computer Methods in Applied Mechanics and Engineering* 397 (2022): 115141.
- [44] Ranade, Rishikesh, Chris Hill, and Jay Pathak. "DiscretizationNet: A machine-learning based solver for Navier–Stokes equations using finite volume discretization." *Computer Methods in Applied Mechanics and Engineering* 378 (2021): 113722.
- [45] Dong X, Chen S, Pan S. Learning to prune deep neural networks via layer-wise optimal brain surgeon. *Advances in neural information processing systems*. 2017;30.
- [46] Spyros Gidaris and Praveer Singh and Nikos Komodakis, Unsupervised Representation Learning by Predicting Image Rotations, 2018, arXiv, <https://doi.org/10.48550/arXiv.1803.07728>